

Sensory and Motor Systems

Activation of Distinct Channelrhodopsin Variants Engages Different Patterns of Network Activity

Na Young Jun¹ and Jessica A. Cardin^{2,3}<https://doi.org/10.1523/ENEURO.0222-18.2019>¹Department of Ophthalmology, Yale University, New Haven, CT 06520, ²Department of Neuroscience, Yale University, New Haven, CT 06520, and ³Kavli Institute for Neuroscience, Yale University, New Haven, CT 06520

Abstract

Several recently developed Channelrhodopsin (ChR) variants are characterized by rapid kinetics and reduced desensitization in comparison to the widely used ChR2. However, little is known about how varying opsin properties may regulate their interaction with local network dynamics. We compared evoked cortical activity in mice expressing three ChR variants with distinct temporal profiles under the CamKII promoter: Chronos, Chrimson, and ChR2. We assessed overall neural activation by measuring the amplitude and temporal progression of evoked spiking. Using γ -range (30–80 Hz) local field potential (LFP) power as an assay for local network engagement, we examined the recruitment of cortical network activity by each tool. All variants caused light-evoked increases in firing *in vivo*, but each demonstrated different temporal patterning of evoked activity. In addition, the three ChRs had distinct effects on cortical γ -band activity. Our findings suggest the properties of optogenetic tools can substantially affect their efficacy *in vivo*, as well their engagement of circuit resonance.

Key words: Channelrhodopsin; Chrimson; Chronos; cortex; γ oscillations; optogenetics

Significance Statement

Genetically modified opsins are some of the most widely used experimental tools in modern neuroscience. However, although these tools are well characterized at the single-cell level, little is known about how the varying properties of the opsins affect their interactions with active neural networks *in vivo*. Here, we present data from experiments using three optogenetic tools with distinct activation/inactivation and kinetic profiles. We find that opsin properties regulate the amplitude and temporal pattern of activity evoked *in vivo*. Despite all evoking elevated spiking, the three opsins also differentially regulate cortical γ oscillations. These data suggest that the kinetic properties of optogenetic tools interact with active neural circuits on several time scales. Optogenetic tool selection should therefore be a key element of experimental design.

Introduction

The advent of easily accessible optogenetic tools for manipulating neural activity has substantially altered experimental neuroscience. The current optogenetics toolkit for neuroscience comprises a large number of Channel-

rhodopsins (ChRs), Halorhodopsins, and Archaelhodopsins that enable activation and suppression of neural activity with millisecond-timescale precision. Within the ChR family, many variants have now been made with altered activation spectra, photocycle kinetics, and ion

Received June 4, 2018; accepted December 1, 2019; First published December 10, 2019.

The authors declare no competing financial interests.

Author contributions: N.Y.J. and J.A.C. designed research; N.Y.J. and J.A.C. performed research; N.Y.J. and J.A.C. analyzed data; N.Y.J. and J.A.C. wrote the paper.

This work was supported by National Institutes of Health Grants R01 MH102365, R01 EY022951, R01 MH113852, and P30 EY026878; a Smith Family Award for Excellence in Biomedical Research; a Klingenstein Fellow-

ship Award; an Alfred P. Sloan Fellowship; a National Alliance for Research on Schizophrenia and Depression Young Investigator Award; a grant from the Ludwig Foundation; and a McKnight Fellowship (J.A.C.).

Acknowledgements: We thank Dr. M.J. Higley for valuable discussions. We thank Dr. E.S. Boyden for generously sharing samples of viral vectors for Chronos and Chrimson used in initial pilot experiments. We thank Mr. Jong Wook Kim for assistance with coding and data analysis.

Correspondence should be addressed to Jessica A. Cardin at jess.cardin@yale.edu.

selectivity. The first tool to be widely used in neuroscientific approaches, ChR2, is a nonspecific cation channel with sensitivity to blue light. ChR2 conferred the ability to evoke action potentials with high precision and reliability across a wide range of cell types (Boyden et al., 2005; Cardin et al., 2009; Deisseroth, 2015). However, the utility of this tool has been somewhat limited by its relatively long offset kinetics and fairly rapid inactivation of photocurrents in response to sustained strong light stimulation (Boyden et al., 2005; Bamann et al., 2008; Ritter et al., 2008; Schoenenberger et al., 2011). In addition, most naturally occurring ChRs are sensitive to blue-green light, presenting a challenge to the use of multiple tools for simultaneous optogenetic control of distinct neural populations. A significant effort in the field has therefore been made to develop ChR variants with faster on- and offset temporal kinetics, less desensitization over time, and red-shifted activation spectra.

Previous work has suggested that the ChRs are highly effective tools for probing the cellular interactions underlying intrinsically generated patterns of brain activity. Stimulation of parvalbumin (PV)-expressing interneurons in the cortex via ChR2 evokes γ oscillations, entrains the firing of excitatory pyramidal neurons, and regulates sensory responses (Cardin et al., 2009; Sohal et al., 2009). Similarly, ChR2 stimulation of PV⁺ GABAergic long-range projection neurons in the basal forebrain generates γ -range oscillations in frontal cortex circuits (Brown and McKenna, 2015). Recent work further suggests that ChR2 activation of Somatostatin-expressing interneurons, which synapse on both PV⁺ cells and excitatory neurons, evokes cortical oscillations in a low γ range (Veit et al., 2017). Sustained depolarization of excitatory sensory cortical neurons via ChR2 activation likewise evokes γ oscillations, likely by engaging reciprocal interactions with local GABAergic interneurons. (Adesnik and Scanziani, 2010). In comparison, activation of pyramidal neurons in mouse motor cortex via ChRGR, another ChR variant, evokes activity in a broad range of lower-band frequencies (Wen et al., 2010). High-fidelity spiking recruited by Chronos, oChIEF, and ReaChR has been used *in vitro* and *in vivo* in visual cortex (Chaigneau et al., 2016; Hass and Glickfeld, 2016; Ronzitti et al., 2017) and the auditory midbrain (Guo et al., 2015; Hight et al., 2015), but the impact of such stimulation on the surrounding network remains unclear.

Despite the substantial increase in available ChR variants with diverse kinetic and spectral properties, it remains unclear how these properties interact with endogenous temporal patterns of neural circuit activity like γ oscillations *in vivo*. Furthermore, the properties of optogenetic tools are typically validated using short pulses of light (1–100 ms) under quiet network conditions *in vitro*, but these tools are widely used for sustained neural activation (100's of ms to

s) under active network conditions *in vivo* (Adesnik and Scanziani, 2010; Bortone et al., 2014; Phillips and Hasenstaub, 2016; Burgos-Robles et al., 2017). Here, we tested the impact of optogenetic tool properties on evoked activity patterns in the intact brain. We took advantage of the well-characterized γ oscillation rhythm in mouse primary visual cortex *in vivo* (Adesnik and Scanziani, 2010; Niell and Stryker, 2010; Vinck et al., 2015) as a metric for optogenetic recruitment of local network activity. Using optogenetic activation of excitatory pyramidal cells as a paradigm to evoke both spiking and cortical γ oscillations, we compared three ChRs with robust photocurrents but distinct kinetic profiles: Chronos, with high-speed on and off kinetics (Klapoetke et al., 2014); ChR2, with fast on but relatively slow off kinetics (Boyden et al., 2005); and Chrimson (Klapoetke et al., 2014), with slow on and off kinetics. We found that these tools, although expressed in the same cell types in the same brain region and effective at eliciting action potentials, evoked distinct patterns of activity and had different effects on γ activity. Together, our data suggest that the kinetic properties of engineered opsin tools affect optogenetic interactions with local circuit activity and should be a key factor in experimental design.

Materials and Methods

Animals

All animal procedures were performed in accordance with the Yale University Institutional Animal Care and Use Committee animal care committee's regulations. We used both female and male C57BL/6J mice ranging from three to five months old.

Surgical procedures

To express ChR2, Chronos, and Chrimson in pyramidal neurons, we injected AAV5-CAMKII-ChR2-GFP (Addgene # 26969), AAV5-CAMKII-CHRONOS-GFP (Addgene # 58805), or AAV5-CAMKII-CHRIMSON-GFP (Addgene # 62718), respectively, in the cortex of C57BL/6J mice. For the virus injection surgery, 1 μ l of AAV was injected through a small burr hole craniotomy in the skull over the left visual cortex (–3.2 mm posterior, –2.5 mm lateral, –500 μ m deep relative to bregma) using a glass pipette. Injections were made via beveled glass micropipette at a rate of ~100 nl/min. After injection, pipettes were left in the brain for ~5 min to prevent backflow. Mice were given four weeks for virus expression before experiments.

Electrophysiological recordings

Mice were anesthetized with 0.3–0.5% isoflurane in oxygen and head-fixed by cementing a titanium headpost to the skull with Metabond (Butler Schein). All scalp incisions were infused with lidocaine. A craniotomy was made over primary visual cortex and electrodes were lowered through the dura into the cortex. All extracellular multiunit (MU) and local field potential (LFP) recordings were made with an array of independently moveable tetrodes mounted in an Eckhorn Microdrive (Thomas Recording). Signals were digitized and recorded by a Digital Lynx system (Neuralynx). All data were sampled at 40

<https://doi.org/10.1523/ENEURO.0222-18.2019>

Copyright © 2020 Jun and Cardin

This is an open-access article distributed under the terms of the Creative Commons Attribution 4.0 International license, which permits unrestricted use, distribution and reproduction in any medium provided that the original work is properly attributed.

kHz. All LFP recordings were referenced to the surface of the cortex (Buzsáki et al., 2012; Herreras, 2016). LFP data were recorded with open filters and MU data were recorded with filters set at 600–9000 Hz.

Optogenetic stimulation was provided via an optical fiber (200 μm) coupled to a laser (Optoengine) at either 470 nm (ChR2 and Chronos stimulation) or 593 nm (Chrimson stimulation). In each experiment, the fiber was placed on the surface of the dura over the virus injection site and the tetrodes were placed immediately posterior to the fiber.

During each experiment, a total of 150 laser pulses (470 or 593 nm) of 1.5-s duration were given at varying light intensities (0.5–10 mW/mm^2) with 10-s interpulse intervals to allow detection of both transient and sustained spiking and LFP activity in response to light pulses. Bouts of 30 pulses were separated by 5-min baseline periods.

Histology

Mice were perfused with 0.1 M PBS followed by 4% PFA in 0.1 M PBS. After perfusion, brains were postfixed for 8 h in 4% PFA. Brains were sliced at 40 μm on a vibratome (Leica) and mounted on slides with DAPI mounting solution (Vector). Initial images were taken with a 10 \times objective on an Olympus microscope and the channels were merged using ImageJ (NIH). Laminar distribution of opsin expression was estimated based on DAPI staining. Confocal images for cell counts were taken with a 64 \times oil objective on a Zeiss LSM 800 confocal microscope. Tissue was stained for NeuN (1:500; MAB377; Millipore) using a red secondary antibody (1:1000; Alexa Fluor Plus 594 goat anti-mouse; Invitrogen). For each mouse, NeuN⁺ cells that were positive and negative for the GFP-tagged opsin were counted in three fields of view in each layer (layers 2/3 and 5).

Data analysis

Data were analyzed using custom scripts written in MATLAB (The MathWorks) and Python. Spikes were detected from the MU recordings using a threshold of +3 SD above the mean, where both the mean and SD were calculated from 10 s of recording preceding any light stimulation. Detected spikes were then used to calculate peristimulus time histogram (PSTH) and raster plots for visualization of optically evoked spiking. For each tetrode recording site, a two-tailed paired *t* test was performed on the firing rates in the prestimulus baseline and during light pulses to determine the presence or absence of a light-evoked change in firing rate. Sites with significant evoked firing rate changes were selected for further analysis. For each recording site, firing rates were normalized to spontaneous firing in the initial prestimulation period and the latency to peak evoked firing after light pulse onset was obtained by selecting the 10-ms interval with the highest spike counts.

Interspike intervals (ISI) were calculated as the time interval between successive spikes, and cumulative distributions of ISIs during the light pulses and spontaneous activity before the light pulses were calculated for each data set. Paired ratio measurements were taken for each light intensity. For measurements of the effect of optoge-

netic stimulation on mean firing rate, we measured the ratio between the prestimulus baseline (1-s period before each light pulse) and evoked firing (1-s period during each light pulse).

Spectrograms of LFP activity were obtained using 400-ms-long Hann windows sliding by 10 ms. Before short-time Fourier transform (STFT), the mean was subtracted to remove DC bias. Each trial was normalized by dividing by the RMS amplitude of the 1-s window preceding onset of the light pulse. Spectrograms were averaged across the LFP responses to 30 pulses of 10 mW/mm^2 of 1.5-s duration. Relative power in the frequency band of interest was then calculated per frequency bin, setting the average power in the first 0.5 s in each bin to be 1. To determine whether optogenetic stimulation changed power in the γ range (30–80 Hz), we compared the average γ power during stimulation at 10 mW/mm^2 with the average γ power during spontaneous activity before the light pulses. To further evaluate the changes in γ -range activity evoked by optogenetic stimulation, we calculated the ratio of the power spectral density in this frequency band during baseline and all stimulation conditions.

The LFP signals included low-amplitude, additive line noise at 60 Hz. The method used by Burns et al. (2010) was not applicable because (1) the amplitude difference caused by the line noise at 60 Hz in the full spectrum was not significant enough, and (2) the 60-Hz line noise was wide-band and leaked to the neighboring frequency bins of the spectrogram as well. Instead, we noticed that the line noise caused a constant phase shift at the 60-Hz line on the spectrogram. The amplitude and phase of the line noise was estimated from the mean value of the complex spectrogram at 60 Hz over all time bins during the 4-s interval, assuming that the true 60-Hz signal coming from LFP would not have a significant phase bias over the period. When we subtracted the estimated line noise from the 60-Hz frequency bin as well as the two neighboring bins, this method effectively eliminated the artifact on the spectrogram coming from the 60-Hz line noise.

Statistics

All analyses were performed on an animal-wise basis throughout, and all data are denoted as mean \pm SEM. For some comparisons, a one-way ANOVA or Kruskal–Wallis test was used, followed by a Dunn's *post hoc* test where appropriate. In cases where nonparametric statistics were appropriate due to non-normal data distributions, a two-tailed Wilcoxon signed-rank test or the Kruskal–Wallis test were used.

Results

Cell type-specific expression of ChRs in mouse visual cortex

To understand the efficacy and utility of recently developed ChR variants with differing kinetic properties, we compared three tools: ChR2, Chronos, and Chrimson (Fig. 1A). We expressed each tool using an AAV construct, under the control of the excitatory neuron-specific CaMKII promoter, into the visual cortex of wild-type mice. Four weeks after virus injection, each of the three ChRs was

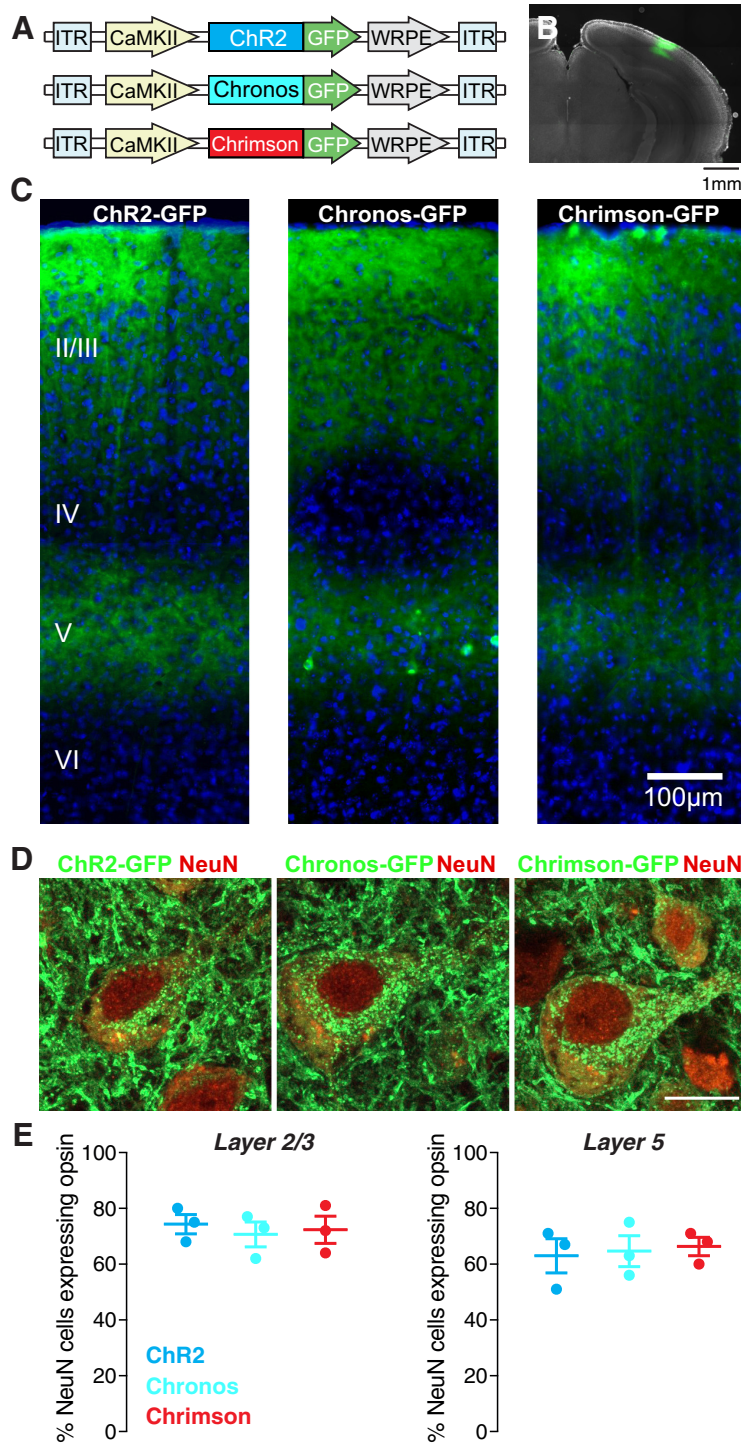


Figure 1. Expression of three ChR variants in excitatory neurons of the mouse visual cortex. **A**, AAVs carrying three opsins were injected into primary visual cortex of wild-type mice; ITR, inverted terminal repeat; WRPE, woodchuck hepatitis B virus post-transcriptional element. **B**, Spread of viral infection in the cortex. Example image showing GFP expression (green) around the area of a cortical injection of AAV5 carrying the Chronos construct. Magnification: 4×. **C**, ChR2-GFP, Chronos-GFP, and Chrimson-GFP were robustly expressed in excitatory neurons in cortical layers 2, 3, and 5, as confirmed by DAPI staining (blue). Magnification: 10×. **D**, Example confocal images showing expression of the three ChR variants (green) in layer 5 pyramidal neurons stained for the neuronal marker NeuN (red). Scale bar: 10 µm. Magnification: 64×. **E**, Quantification of expression in layers 2/3 (left) and 5 (right) for each opsin.

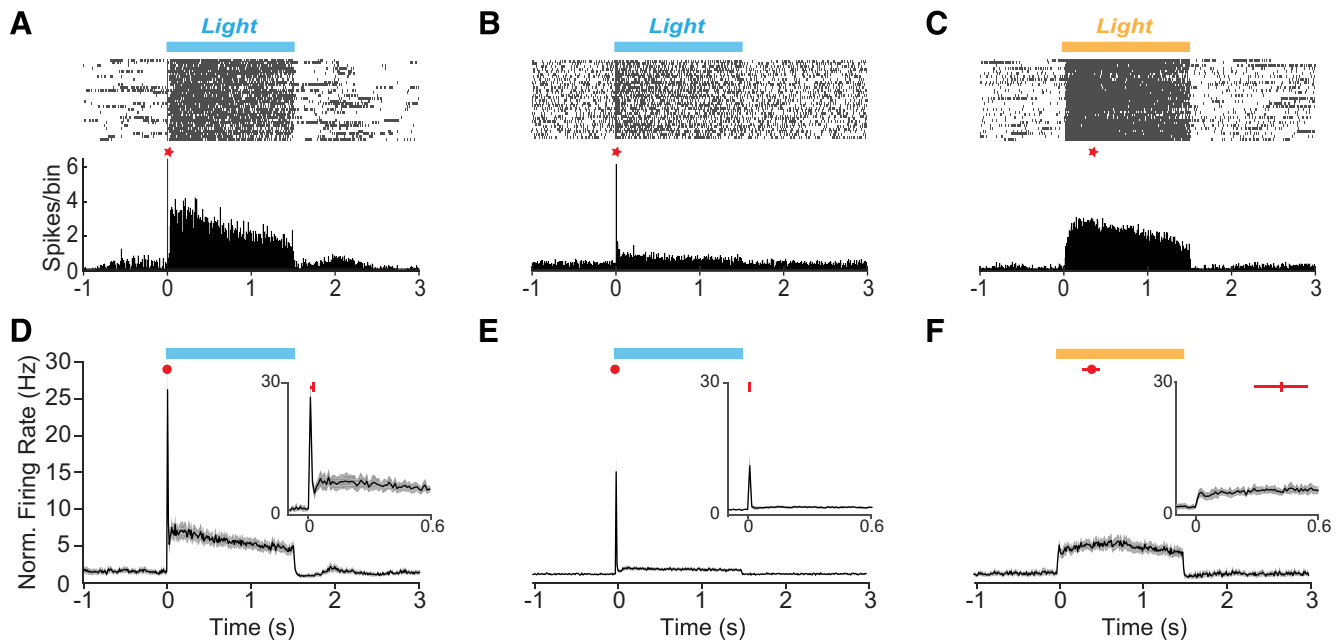


Figure 2. Different ChRs evoke cortical activity with distinct temporal profiles *in vivo*. **A**, Raster plots (upper) and histograms (lower) of example MU spike activity during stimulation of excitatory pyramidal neurons with ChR2. The 1.5-s-long interval of light stimulation (10 mW/mm^2) is indicated as shaded box. An asterisk indicates the peak firing evoked by the light pulse. **B**, Same as in **A**, for Chronos. **C**, Same as in **A**, for Chrimson. **D**, Average PSTH for all recorded sites in ChR2-expressing mice. Red symbols and lines indicate the mean peak time and SEM of the peak time, respectively. Inset shows the initial period of evoked firing in the first 600 ms of light stimulation. **E**, Same as in **D**, for Chronos. **F**, Same as in **D**, for Chrimson.

robustly expressed in a characteristic distribution of excitatory pyramidal neurons in cortical layers 2/3, 5, and 6 (Fig. 1C; Longson et al., 1997; Cardin et al., 2009). In each case, opsin expression was widespread in visual cortex, covering a distance of up to $410 \mu\text{m}$ from the initial injection site (Fig. 1B). To quantify the expression of each opsin, we performed confocal microscopy of tissue co-stained for the neuronal marker NeuN (Fig. 1D). We observed similar numbers of opsin-expressing neurons in layers 2/3 and 5 across all three groups of animals (layer 2/3: ChR2 $74.3 \pm 3.5\%$, Chronos $70.7 \pm 4.5\%$, Chrimson $72.3 \pm 4.9\%$; Kruskal–Wallis test $p = 0.87$, $dF = 2$, $H = 0.36$; layer 5: ChR2 $63 \pm 6.1\%$, Chronos $64.7 \pm 5.5\%$, Chrimson $66.3 \pm 3.3\%$; $p = 0.92$, $dF = 2$, $H = 0.2$; Fig. 1E).

Different ChRs evoke distinct cortical activity profiles *in vivo*

The temporal profile of circuit activity evoked by different opsins may differentially engage network dynamics. To assess the initial and sustained levels of spiking evoked by each opsin, we recorded population MU and LFP activity at multiple cortical sites around each viral injection (ChR2: 18 sites in six animals, Chronos: 11 sites in five animals, Chrimson: 15 sites in six animals). Spontaneous firing rates did not differ among the three groups of animals (ChR2: 37.7 ± 5.4 , Chronos: 72.8 ± 21.32 , Chrimson: 42.9 ± 7.4 ; one-way AVOVA, $p = 0.14$, $dFn = 2$, $dFd = 14$, $F = 2.28$).

When stimulated with 1.5 s of continuous light in an appropriate wavelength (10 mW/mm^2 , wavelength: 470 nm for ChR2 and Chronos, 593 nm for Chrimson), all three ChRs evoked sustained firing (Fig. 2A–C). However, each opsin was associated with a distinct temporal profile of

spiking. Whereas stimulation of ChR2-expressing (Fig. 2A,D) or Chrimson-expressing (Fig. 2C,F) neurons evoked sustained firing over ~ 1 –2 s, stimulation of Chronos-expressing neurons generated strong initial spiking followed by a decrease toward baseline firing levels (Fig. 2B,E). The peak firing evoked by ChR2 and Chronos was rapid and reliable, whereas the peak firing achieved by Chrimson stimulation was delayed and highly variable (Fig. 2D–F, inset panels).

To quantify these differences in temporal kinetics induced by the three ChR variants, we compared the time between the light pulse onset and the center of the 10 ms interval with the most frequent spikes, averaged over all recording sites and mice for each ChR variant. Chronos showed the shortest peak latency of $0.005 \pm 0.001 \text{ s}$, whereas Chrimson had a peak latency of $0.42 \pm 0.13 \text{ s}$, compared to ChR2 at $0.01 \pm 0.01 \text{ s}$. (Fig. 2D–F; Kruskal–Wallis test; $p = 0.0015$, $dF = 2$, $H = 10.74$). The latency to peak was longer for Chrimson, but not Chronos, compared to ChR2 (Dunn’s *post hoc* test; $p = 0.04$, $p = 0.75$).

To assay the efficacy of each optogenetic tool in engaging local cortical neurons, we compared the recruitment of spikes in response to a range of low illumination intensities. We examined the difference in spike timing between spontaneous firing and optogenetic stimulation periods by comparing the distributions of ISIs evoked by activation of ChR2, Chronos, and Chrimson (Fig. 3). ChR2 (Fig. 3A) and Chrimson (Fig. 3C) both evoked a robust decrease in ISI, consistent with the sustained increase in firing rate, whereas activation of Chronos (Fig. 3B) had only a modest effect on the overall ISI distribution. ChR2-expressing (Fig. 3D) and Chrimson-expressing (Fig. 3F)

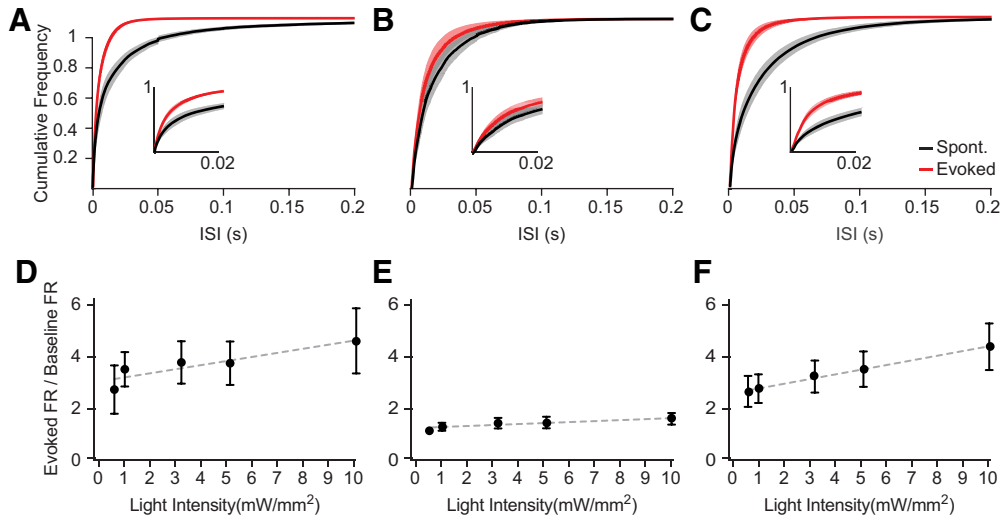


Figure 3. Amplitude and frequency distribution of evoked spike response varies with optogenetic tool. **A**, ISIs of spontaneous (black) and evoked (red) MU activity during optogenetic stimulation (10 mW/mm²) in ChR2-expressing cortex. Inset shows an enlarged plot of the initial 200 ms of the evoked spike response. **B**, Same as in **A**, for Chronos. **C**, Same as in **A**, for Chrimson. Error bars denote SEM. **D**, Firing rates evoked by ChR2 stimulation over a range of intensities, divided by baseline spontaneous firing immediately before the light pulses. **E**, Same as in **D**, for Chronos. **F**, Same as in **D**, for Chrimson. Dashed lines indicate linear regression of the data. Error bars denote SEM.

mice showed increasing evoked spiking as the light stimulation intensity increased (linear regression slopes: ChR2 = 0.16 ± 0.04 , $r^2 = 0.82$, $p = 0.04$, $dFn = 1$, $dFd = 3$, $F = 13.56$; Chrimson = 0.18 ± 0.01 , $r^2 = 0.9$, $p < 0.0001$, $dFn = 1$, $dFd = 3$, $F = 969.1$). However, mean firing rates evoked by Chronos activation did not increase with light intensity (linear regression slope: 0.04 ± 0.01 , $r^2 = 0.99$, $p = 0.01$, $dFn = 1$, $dFd = 3$, $F = 28.1$). Restricting analysis to the first 100 ms of the stimulation period revealed the decreased ISIs initially evoked by all three opsins (Fig. 4A–C). However, the profiles of evoked firing responses

across increasing light intensities were similar to those observed in the full analysis shown in Figure 3D–F (linear regression slope: ChR2 = 0.26 ± 0.1 , $r^2 = 0.67$, $p = 0.09$, $dFn = 1$, $dFd = 3$, $F = 6.02$; Chrimson = 0.16 ± 0.07 , $r^2 = 0.91$, $p = 0.09$, $dFn = 1$, $dFd = 3$, $F = 29.2$; Chronos = 0.036 ± 0.007 , $r^2 = 0.66$, $p = 0.01$, $dFn = 1$, $dFd = 3$, $F = 5.91$; Fig. 4D–F).

Opsin-specific recruitment of cortical γ rhythms

Previous work has found that ChR2 stimulation of pyramidal neurons engages the cortical γ rhythm (30–80

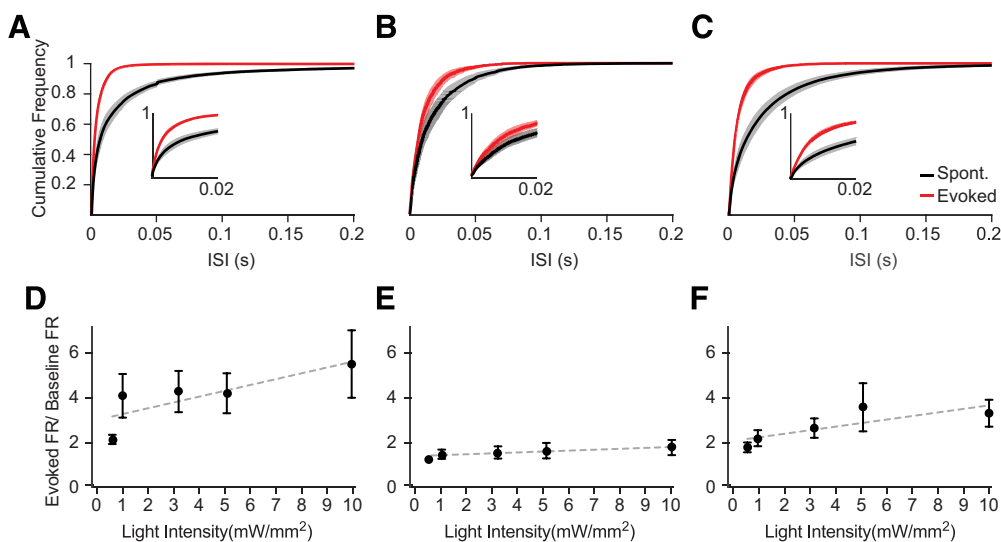


Figure 4. Distinct changes in evoked spike patterns during the first 100 ms after light onset. **A**, ISIs of spontaneous (black) and evoked (red) MU activity during the initial 100 ms of optogenetic stimulation (10 mW/mm²) in ChR2-expressing cortex. **B**, Same as in **A**, for Chronos. **C**, Same as in **A**, for Chrimson. Error bars denote SEM. **D**, Firing rates evoked by the initial 100 ms of ChR2 stimulation over a range of intensities, divided by baseline spontaneous firing rates immediately before the light pulses. **E**, Same as in **D**, for Chronos. **F**, Same as in **D**, for Chrimson. Dashed lines indicate linear regression of the data. Error bars denote SEM.

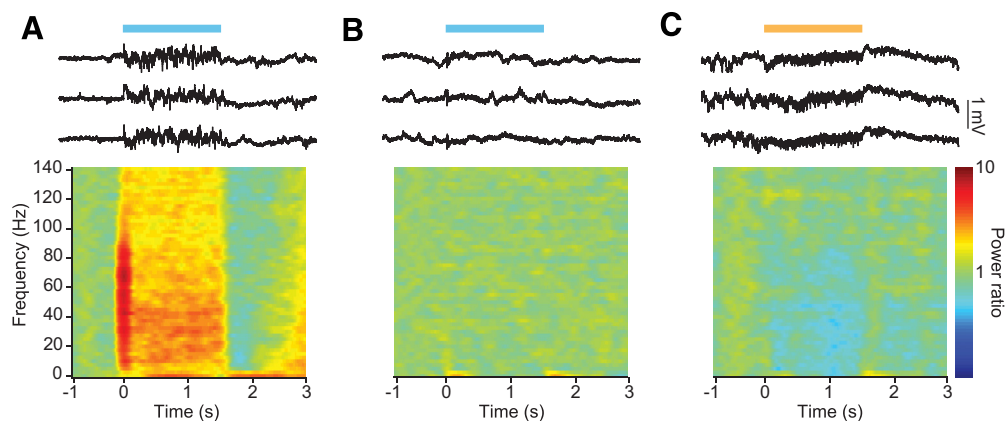


Figure 5. Different ChRs evoke distinct cortical activity profiles *in vivo*. **A**, Example traces of cortical LFP activity in response to 1.5 s of 10 mW/mm² light stimulation of ChR2-expressing pyramidal neurons (upper). Average changes in spectral power density at this site across stimulation trials (lower). **B**, Same as in **A**, for Chronos. **C**, Same as in **A**, for Chrimson.

Hz), an outcome of resonant excitatory-inhibitory circuit interactions (Cardin, 2016), *in vitro* and *in vivo* (Adesnik and Scanziani, 2010). Using evoked γ power as a measure of network activation, we assayed the efficacy of each optogenetic tool in driving recurrent circuit interactions. Activation of ChR2-expressing excitatory neurons evoked a response in the LFP and a broadband increase in high-frequency activity centered around the γ band (Fig. 5A). Chronos and Chrimson likewise evoked an initial deflection of the LFP signal (Fig. 5B,C). However, neither Chronos nor Chrimson activation of excitatory neurons evoked the characteristic sustained high-frequency LFP activity observed following ChR2 stimulation of the same population of neurons.

In agreement with previous work (Adesnik and Scanziani, 2010), we found that the light-activation of ChR2-expressing excitatory neurons amplified LFP power in the γ range ($p = 0.03$, $W = 19$; Wilcoxon signed-rank test; Fig. 6A,D). In contrast, neither Chrimson nor Chronos demonstrated similar engagement of endogenous patterns of cortical network activity during stimulation. Stimulation of excitatory neurons via activation of Chronos had little effect on γ power ($p = 0.23$, $W = -8$; Fig. 6B,E). Surprisingly, excitatory neuron stimulation via Chrimson significantly suppressed cortical power across a range of high frequencies, including the γ band, in a light-intensity-dependent manner ($p = 0.023$, $W = -15$; Figs. 5C, 6C,F). Together, these data suggest that the pattern of activity recruited by stimulation with these three different tools engages distinct modes of endogenous circuit interactions.

Discussion

Although recent work has resulted in the development of new ChR variants to meet experimental needs, the *in vivo* effects of opsins with distinct properties have not been fully explored. In particular, varying temporal profiles of optogenetically evoked neural activation may substantially affect the manner in which the surrounding neural circuit is engaged. Here, we expressed three opsins (ChR2, Chronos, and Chrimson) with different kinetics in excitatory pyramidal neurons in the primary visual cortex. Using a

previously validated paradigm for optogenetic recruitment of γ -range resonance in the local cortical circuit, we compared the temporal envelope of evoked spiking and γ -range activity across the three opsins. Although all three tools were effective in driving enhanced spiking, the temporal profile of the evoked activity was distinct. In addition, only ChR2 stimulation generated increased cortical γ activity.

Recently developed ChRs vary extensively in their kinetic profiles. ChR2 exhibits a relatively fast onset (τ_{on}) but a long offset time (τ_{off}), leading to diminished temporal fidelity in spike responses (Gunaydin et al., 2010). The τ_{off} of several ChRs also slows further on membrane depolarization (Mattis et al., 2011). The cumulative effect of this long τ_{off} is to cause a prolonged depolarization after the evoked action potential, preventing rapid re-hyperpolarization of the membrane and contributing to artificial spike doublets. Prolonged depolarization may also inactivate voltage-gated channels needed for high-frequency spiking. In comparison, Chronos exhibits large photocurrents, rapid deactivation, and improved efficacy in eliciting high-fidelity fast spiking (Lin et al., 2009; Klapoetke et al., 2014).

Another recent series of tools were developed with absorption spectra shifted toward longer wavelengths compatible with two-photon imaging (Packer et al., 2012; Prakash et al., 2012; Agetsuma et al., 2017) and dual-channel optogenetic circuit interrogation. Chrimson exhibits a red-shifted absorption peak and very large photocurrents, making it highly effective for driving robust neural activity (Klapoetke et al., 2014). Chrimson has substantially slower τ_{on} and τ_{off} properties than ChR2, Chronos, ReaChR, or bReaCHES (Yizhar et al., 2011; Lin et al., 2013; Klapoetke et al., 2014; Rajasethupathy et al., 2015). Based on their low toxicity, robust expression levels, large peak photocurrents, and distinct kinetic profiles, we selected Chronos and Chrimson for *in vivo* comparison with ChR2.

We found a strong relationship between the properties of the individual opsins and the temporal profile of the spiking they evoked. The two tools with relatively rapid onset kinetics, ChR2 and Chronos, each evoked a pre-

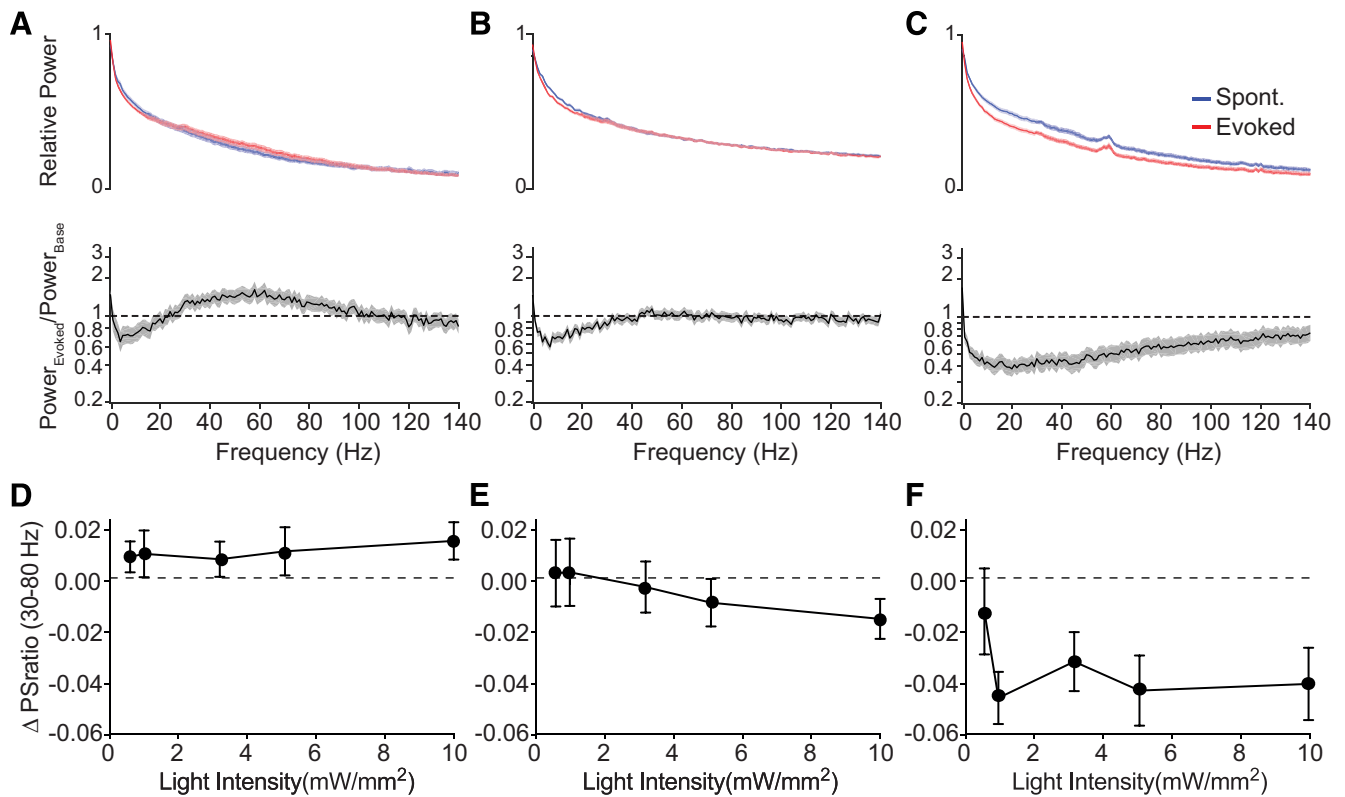


Figure 6. Distinct recruitment of γ -band activity by different ChRs. **A**, Normalized power spectra (upper) for spontaneous (blue) and evoked (red) cortical LFP activity in response to ChR2 stimulation, averaged across all stimulation levels, and the ratio between evoked and spontaneous spectra (lower). **B**, Same as in **A**, for Chronos. **C**, Same as in **A**, for Chrimson. Shaded areas denote \pm SEM. **D**, Change in the relative power in the γ band (30–80 Hz) in response to varying light intensities in cortex expressing ChR2. **E**, Same as in **D**, for Chronos. **F**, Same as in **D**, for Chrimson. Error bars denote SEM.

cisely timed initial spike event across the neuronal population, followed by sustained spiking at lower firing rates. In contrast, Chrimson, with slow onset kinetics, did not evoke reliable spiking at stimulation onset and gave rise to a much broader temporal distribution of spike frequencies. These results, along with previous findings (Mattis et al., 2011; Schoenenberger et al., 2011), suggest that the kinetics of the opsins interact meaningfully with intrinsic neuronal membrane properties to affect the temporal pattern of evoked spiking. Rapid membrane depolarization, like that caused by ChR2 or Chronos activation, contributes to recruitment of voltage-gated channels and enhances the reliability and precision of the initial evoked action potentials in cortical neurons (Wilent and Contreras, 2005; Cardin et al., 2010). In comparison, a slow rate of depolarization, like that caused by Chrimson, leads to temporally dispersed spiking. We further found that the kinetics of the opsins shaped the overall temporal envelope of the sustained spiking evoked by long stimulation. Whereas the initial efficacy of ChR2 and Chronos resulted in an early peak in evoked firing rates within the first 50 ms, the spike response to Chrimson stimulation peaked several hundred milliseconds later. However, the sustained firing rates evoked by ChR2 and Chrimson were higher than that evoked by Chronos, suggesting that rapid deactivation of this opsin may reduce overall spike rates.

Gamma oscillations are generated by reciprocal, rhythmic interactions between excitatory and inhibitory neurons (Cardin, 2016). Gamma activity in cortical circuits can be evoked by optogenetically stimulating either the inhibitory interneurons (Cardin et al., 2009; Sohal et al., 2009; Veit et al., 2017) or the excitatory neurons (Adesnik and Scanziani, 2010; Lu et al., 2015). Generation of γ oscillations by excitatory neuron stimulation likely results from the highly synchronous activation of a large volley of spikes from excitatory neurons, which are particularly effective in activating the inhibitory neuron spiking that sets the temporal pattern for resonance in the network (Cardin et al., 2009; Sohal et al., 2009; Buzsáki and Wang, 2012; Cardin, 2016). Several cycles of γ can be produced by even a single brief stimulation of excitatory pyramidal neurons (Sohal et al., 2009), but sustained γ oscillations in active cortical networks *in vivo* may require consistently elevated excitatory spiking (Brunel and Wang, 2003; Buzsáki and Wang, 2012). Given these temporal constraints, the different temporal profiles of evoked excitatory neuron spiking evoked by the three ChRs could potentially engage varying network responses.

In good agreement with previous work (Adesnik and Scanziani, 2010), we found that ChR2 stimulation of excitatory pyramidal neurons evokes robust cortical γ activity. In contrast, stimulation of the same neuronal population via Chronos evoked little to no γ activity, pre-

sumably because the initial, highly precise spiking from stimulated cells is not followed by sufficiently elevated excitatory spiking to sustain network oscillations. In comparison, Chrimson might be expected to evoke little γ because the slow increase in activity precludes an initial burst of spikes. Surprisingly, we found that stimulation via Chrimson also significantly suppressed endogenous power in a broad range of high frequencies, including the γ band. These results suggest that Chrimson's slow temporal kinetics and late firing peak destabilize the highly precise interplay between E and I cells, increasing the firing rates of excitatory neurons but broadly disrupting high-frequency activity and precluding rhythmic entrainment by inhibition. Because the impact of optogenetic drive to interneurons on oscillatory activity may vary with behavioral state (Veit et al., 2017), further work may be necessary to determine whether these findings, obtained under a low level of anesthesia, extend to other states such as wakefulness.

Overall, we found that differences in the properties of three ChRs were associated with distinct profiles of evoked cortical activity. Although this does not represent an exhaustive evaluation of all available opsins, our data suggest that the temporal properties of the opsins affect the temporal profile of evoked activity on multiple time scales. Rapid onset kinetics may facilitate the recruitment of highly precise initial spike responses, whereas slow onset kinetics preclude synchronous spiking and result in delayed peak responses. In addition, opsins with distinct kinetics interact differently with endogenous circuit resonance, affecting the sustained patterns of activity evoked in cortical networks over longer time periods. Our findings suggest complex interactions between optogenetic tools and active neuronal networks in the intact brain. The optogenetics toolkit for neuroscience includes an ever-increasing variety of tools with varying properties, and individual tools may be appropriate for different experimental goals.

References

- Adesnik H, Scanziani M (2010) Lateral competition for cortical space by layer-specific horizontal circuits. *Nature* 464:1155–1160.
- Agetsuma M, Hamm JP, Tao K, Fujisawa S, Yuste R (2017) Parvalbumin-positive interneurons regulate neuronal ensembles in visual cortex. *Cereb Cortex* 28:1831–1845.
- Bamann C, Kirsch T, Nagel G, Bamberg E (2008) Spectral characteristics of the photocycle of channelrhodopsin-2 and its implication for channel function. *J Mol Biol* 375:686–694.
- Bortone DS, Olsen SR, Scanziani M (2014) Translaminar inhibitory cells recruited by layer 6 corticothalamic neurons suppress visual cortex. *Neuron* 82:474–485.
- Boyden ES, Zhang F, Bamberg E, Nagel G, Deisseroth K (2005) Millisecond-timescale, genetically targeted optical control of neural activity. *Nat Neurosci* 8:1263–1268.
- Brown RE, McKenna JT (2015) Turning a negative into a positive: ascending GABAergic control of cortical activation and arousal. *Front Neurol* 6:135.
- Brunel N, Wang XJ (2003) What determines the frequency of fast network oscillations with irregular neural discharges? I. Synaptic dynamics and excitation-inhibition balance. *J Neurophysiol* 90:415–430.
- Burgos-Robles A, Kimchi EY, Izadmehr EM, Porzenheim MJ, Ramos-Guasp WA, Nieh EH, Felix-Ortiz AC, Namburi P, Leppla CA, Presbrey KN, Anandalingam KK, Pagan-Rivera PA, Anahtar M, Beyeler A, Tye KM (2017) Amygdala inputs to prefrontal cortex guide behavior amid conflicting cues of reward and punishment. *Nat Neurosci* 20:824–835.
- Burns SP, Xing D, Shelley MJ, Shapley RM (2010) Searching for auto-coherence in the cortical network with a time-frequency analysis of the local field potential. *J Neurosci* 30:4033–4047.
- Buzsáki G, Wang XJ (2012) Mechanisms of gamma oscillations. *Annu Rev Neurosci* 35:203–225.
- Buzsáki G, Anastassiou CA, Koch C (2012) The origin of extracellular fields and currents—EEG, ECoG, LFP and spikes. *Nat Rev Neurosci* 13:407–420.
- Cardin JA (2016) Snapshots of the brain in action: local circuit operations through the lens of γ oscillations. *J Neurosci* 36:10496–10504.
- Cardin JA, Carlén M, Meletis K, Knoblich U, Zhang F, Deisseroth K, Tsai LH, Moore CI (2009) Driving fast-spiking cells induces gamma rhythm and controls sensory responses. *Nature* 459:663–667.
- Cardin JA, Kumbhani RD, Contreras D, Palmer LA (2010) Cellular mechanisms of temporal sensitivity in visual cortex neurons. *J Neurosci* 30:3652–3662.
- Chaigneau E, Ronzitti E, Gajowa MA, Soler-Llavina GJ, Tanese D, Brureau AY, Papagiakoumou E, Zeng H, Emiliani V (2016) Two-photon holographic stimulation of ReaChR. *Front Cell Neurosci* 10:234.
- Deisseroth K (2015) Optogenetics: 10 years of microbial opsins in neuroscience. *Nat Neurosci* 18:1213–1225.
- Gunaydin LA, Yizhar O, Berndt A, Sohal VS, Deisseroth K, Hegemann P (2010) Ultrafast optogenetic control. *Nat Neurosci* 13:387–392.
- Guo W, Hight AE, Chen JX, Klapeotke NC, Hancock KE, Shinn-Cunningham BG, Boyden ES, Lee DJ, Polley DB (2015) Hearing the light: neural and perceptual encoding of optogenetic stimulation in the central auditory pathway. *Sci Rep* 5:10319.
- Hass CA, Glickfeld LL (2016) High-fidelity optical excitation of cortico-cortical projections at physiological frequencies. *J Neurophysiol* 116:2056–2066.
- Herreras O (2016) Local field potentials: myths and misunderstandings. *Front Neural Circuits* 10:101.
- Hight AE, Kozin ED, Darrow K, Lehmann A, Boyden E, Brown MC, Lee DJ (2015) Superior temporal resolution of Chronos versus channelrhodopsin-2 in an optogenetic model of the auditory brainstem implant. *Hear Res* 322:235–241.
- Klapeotke NC, Murata Y, Kim SS, Pulver SR, Birdsey-Benson A, Cho YK, Morimoto TK, Chuong AS, Carpenter EJ, Tian Z, Wang J, Xie Y, Yan Z, Zhang Y, Chow BY, Surek B, Melkonian M, Jayaraman V, Constantine-Paton M, Wong GK, et al. (2014) Independent optical excitation of distinct neural populations. *Nat Methods* 11:338–346.
- Lin JY, Lin MZ, Steinbach P, Tsien RY (2009) Characterization of engineered channelrhodopsin variants with improved properties and kinetics. *Biophys J* 96:1803–1814.
- Lin JY, Knutsen PM, Muller A, Kleinfeld D, Tsien RY (2013) ReaChR: a red-shifted variant of channelrhodopsin enables deep transcranial optogenetic excitation. *Nat Neurosci* 16:1499–1508.
- Longson D, Longson CM, Jones EG (1997) Localization of CAM II kinase-alpha, GAD, GluR2 and GABA(A) receptor subunit mRNAs in the human entorhinal cortex. *Eur J Neurosci* 9:662–675.
- Lu Y, Truccolo W, Wagner FB, Vargas-Irwin CE, Ozden I, Zimmermann JB, May T, Agha NS, Wang J, Nurmikko AV (2015) Optogenetically induced spatiotemporal gamma oscillations and neuronal spiking activity in primate motor cortex. *J Neurophysiol* 113:3574–3587.
- Mattis J, Tye KM, Ferenczi EA, Ramakrishnan C, O'Shea DJ, Prakash R, Gunaydin LA, Hyun M, Fenno LE, Gradinaru V, Yizhar O, Deisseroth K (2011) Principles for applying optogenetic tools derived from direct comparative analysis of microbial opsins. *Nat Methods* 9:159–172.
- Niell CM, Stryker MP (2010) Modulation of visual responses by behavioral state in mouse visual cortex. *Neuron* 65:472–479.

- Packer AM, Peterka DS, Hirtz JJ, Prakash R, Deisseroth K, Yuste R (2012) Two-photon optogenetics of dendritic spines and neural circuits. *Nat Methods* 9:1202–1205.
- Phillips EA, Hasenstaub AR (2016) Asymmetric effects of activating and inactivating cortical interneurons. *Elife* 5:e18383.
- Prakash R, Yizhar O, Grewe B, Ramakrishnan C, Wang N, Goshen I, Packer AM, Peterka DS, Yuste R, Schnitzer MJ, Deisseroth K (2012) Two-photon optogenetic toolbox for fast inhibition, excitation and bistable modulation. *Nat Methods* 9:1171–1179.
- Rajasethupathy P, Sankaran S, Marshel JH, Kim CK, Ferenczi E, Lee SY, Berndt A, Ramakrishnan C, Jaffe A, Lo M, Liston C, Deisseroth K (2015) Projections from neocortex mediate top-down control of memory retrieval. *Nature* 526:653–659.
- Ritter E, Stehfest K, Berndt A, Hegemann P, Bartl FJ (2008) Monitoring light-induced structural changes of channelrhodopsin-2 by UV-visible and Fourier transform infrared spectroscopy. *J Biol Chem* 283:35033–35041.
- Ronzitti E, Conti R, Zampini V, Tanese D, Foust AJ, Klapoetke N, Boyden ES, Papagiakoumou E, Emiliani V (2017) Submillisecond optogenetic control of neuronal firing with two-photon holographic photoactivation of chronos. *J Neurosci* 37:10679–10689.
- Schoenenberger P, Schärer YP, Oertner TG (2011) Channelrhodopsin as a tool to investigate synaptic transmission and plasticity. *Exp Physiol* 96:34–39.
- Sohal VS, Zhang F, Yizhar O, Deisseroth K (2009) Parvalbumin neurons and gamma rhythms enhance cortical circuit performance. *Nature* 459:698–702.
- Veit J, Hakim R, Jadi MP, Sejnowski TJ, Adesnik H (2017) Cortical gamma band synchronization through somatostatin interneurons. *Nat Neurosci* 20:951–959.
- Vinck M, Batista-Brito R, Knoblich U, Cardin JA (2015) Arousal and locomotion make distinct contributions to cortical activity patterns and visual encoding. *Neuron* 86:740–754.
- Wen L, Wang H, Tanimoto S, Egawa R, Matsuzaka Y, Mushiake H, Ishizuka T, Yawo H (2010) Opto-current-clamp actuation of cortical neurons using a strategically designed channelrhodopsin. *PLoS One* 5:e12893.
- Wilentz WB, Contreras D (2005) Stimulus-dependent changes in spike threshold enhance feature selectivity in rat barrel cortex neurons. *J Neurosci* 25:2983–2991.
- Yizhar O, Fenno LE, Prigge M, Schneider F, Davidson TJ, O’Shea DJ, Sohal VS, Goshen I, Finkelstein J, Paz JT, Stehfest K, Fudim R, Ramakrishnan C, Huguenard JR, Hegemann P, Deisseroth K (2011) Neocortical excitation/inhibition balance in information processing and social dysfunction. *Nature* 477:171–178.